PCCP

PAPER

View Article Online
View Journal | View Issue

Cite this: *Phys. Chem. Chem. Phys.*, 2018, **20**, 17859

Iodine binding with thiophene and furan based dyes for DSCs†

Alexandra Baumann, ‡[a] Hammad Cheema, ‡[a] Md Abdus Sabuj,[b] Louis E. McNamara,[a] Yanbing Zhang,[a] Adithya Peddapuram,[a] Suong T. Nguyen,[a] Davita L. Watkins,[a] Nathan I. Hammer,[a] Neeraj Rai[b] and Jared H. Delcamp *[a]

Received 14th May 2018,
Accepted 8th June 2018

DOI: 10.1039/c8cp03065k

rsc.li/pccp

Iodine binding to thiophene rings in dyes for dye-sensitized solar cells (DSCs) has been hypothesized to be performance degrading in a number of literature cases. Binding of iodine to dyes near the semiconductor surface can promote undesirable electron transfers and lower the overall efficiency of devices. Six thiophene or furan containing dye analogs were synthesized to analyze iodine binding to the dyes *via* Raman spectroscopy, UV-Vis studies, device performance metrics and density functional theory (DFT) based computations. Evidence suggests I_2 binds thiophene-based dyes stronger than furan-based dyes. This leads to higher DSC device currents and voltages from furan analogues, and longer electron lifetimes in DSC devices using furan based dyes. Raman spectrum of the TiO_2 surface-bound dyes reveals additional and more instense peaks for thiophene dyes in the presence of I_2 relative to no I_2. Additionally, broader and shifted UV-Vis peaks are observed for thiophene dyes in the presence of I_2 on TiO_2 films suggesting significant interaction between the dye molecules and I_2. These observations are also supported by DFT and TD-DFT calculations which indicate the absence of a key geometric energy minimum in the dye–I_2 ground state for furan dyes which are readily observed for the thiophene based analogues.

Introduction

The need for an energy source that is both sustainable and renewable is apparent. One viable option that is cost-effective and potentially aesthetically appealing are dye-sensitized solar cells (DSCs).[1,2] DSC devices operate by: (1) photoexcitation of a dye molecule, (2) injection of excited electrons into a semiconductor conduction band (*e.g.* TiO_2 CB), (3) an electron traversing an external circuit to the counter electrode, (4) collection of the electron at the counter electrode by a redox shuttle, and finally (5) transfer of the electron from the redox shuttle to the oxidized dye molecule.[3] Organic dye based DSCs have been able to reach power conversion efficiencies (PCEs) for this process in excess of 14%, but there is still room for improvement by minimizing non-productive electron transfers such as from TiO_2 to the dye (back electron transfer) or from TiO_2 to the redox shuttle (recombination).[4–6] Undesirable charge recombinations are thought to increase when the iodine (I_2) redox shuttle binds with a dye near the TiO_2 surface (Fig. 1).[7–10] Minimizing recombination events which prevent electrons from completing an external circuit is critical to developing higher efficiency DSC devices.

Isothiocyanates (NCS) bound to transition metals, amine, cyano, halide and thioether groups have been demonstrated to bind iodine and iodide through prior spectroscopic, computational and device studies.[9–21] Despite good evidence of sulfur-based NCS groups and aromatic 5-member heterocycle selenophenes[8] interacting with iodine, experimental evidence of thiophenes binding I_2 is lacking. However, thiophene is

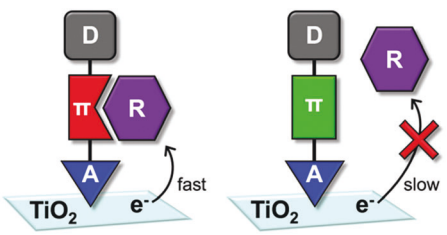

Fig. 1 Example of a D–π–A dye binding a redox shuttle "R" near the TiO_2 surface (left) and a dye with no redox shuttle binding (right).

[a] Department of Chemistry and Biochemistry, University of Mississippi, University, MS 38677, USA. E-mail: delcamp@olemiss.edu
[b] Dave C. Swalm School of Chemical Engineering and Center for Advanced Vehicular Systems, Mississippi State University, Mississippi State, MS 39762, USA

† Electronic supplementary information (ESI) available: With optical and electrochemical characterization, NMR spectrum, and computational Cartesian coordinates. See DOI: 10.1039/c8cp03065k

‡ Indicates authors contributed equally.

commonly implicated in promoting recombination by binding I_2 near the semiconductor surface.[22,23] Several computational reports suggest thiophene-based dyes binding I_2 may be favorable and likely has device performance implications.[18,24–27] The possibility of thiophene binding I_2 is concerning since thiophenes have become ubiquitous in DSC organic-dye design. To probe the ongoing hypothesis that I_2 in DCSs is binding to the sulfur atom present in thiophene stronger than the oxygen atom present in furan rings, we have systematically studied a series of six thiophene or furan based-dye analogs experimentally *via* Raman spectroscopy, UV-Vis absorption, and DSC device performance properties, as well as computationally *via* geometry analysis, binding strength comparisons, and analysis of vertical transition events. The results put forward in this manuscript offer strong evidence of thiophenes binding I_2 which leads to lower DSC device performances.

We hypothesized sulfur would bind I_2 stronger than oxygen due to the higher polarizability of sulfur which is more similar to iodine.[28] Additionally, the widened C–S–C angle of thiophene relative to the C–O–C angle of furan could play an important role in accessibility of the S atom to I_2. To test this, we employed dyes in our studies which replace a thiophene ring with a furan ring to give a single atom change within the larger dye structure. Donor and π-bridge functionality was examined for three sets of dyes which all employ the ubiquitous cyanoacrylic acid acceptor within the donor–π bridge–acceptor (D–π–A) framework. Specifically, **LD03** (thiophene) and **LD04** (furan) have a simple alkyl ether donor group as part of the D–π–A conjugated system (Fig. 2). This limits the heteroatom (non-carbon or hydrogen) binding positions relative to more complex dye systems. Hagfeldt's triarylamine donor was used to compare dyes varying π-bridges from one thiophene (**D35**), one furan (**AB3**), two thiophenes (**AB1**), and one thiophene with one furan (**AB2**) (Fig. 2). This donor was selected as **D35** has been extensively studied and allows for a comparison to an established dye. The target dyes were known (**AB1**, **LD03** and **LD04**),[29,30] commercially available (**D35** *via* Dyenamo), or prepared through analogous routes to the thiophene analogues[29,31] for the unknown furan dyes (**AB2** and **AB3**, see Scheme S1, ESI† for synthetic route).

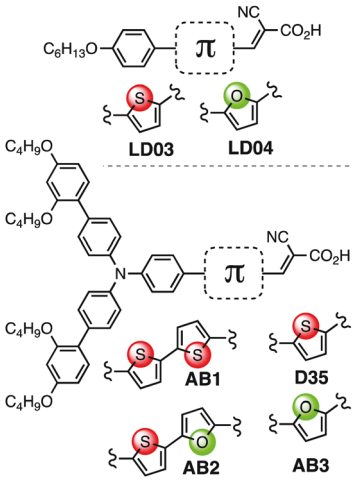

Fig. 2 Target structures of **AB1**, **AB2**, **AB3**, **D35**, **LD03** and **LD04** dyes.

Results and discussion

Raman spectroscopy

First, we examined the vibrational spectrum of the dyes with and without I_2 present on TiO_2 films in acetonitrile (MeCN) *via* Raman spectroscopy. Raman spectroscopy provides a sensitive spectroscopic method for evaluation of dye vibrational modes under conditions similar to those in devices for the neutral ground-state dye at a surface in the presence of MeCN with and without I_2. If iodine binding were to occur to the sulfur atom stronger than oxygen, we reasoned a change in the vibrational spectra of the dye molecules would be expected due to new vibrational peaks resulting from new vibrational modes associated with a S–I_2 binding or a change in the relative intensity of already existing peaks by perturbation of ring breathing/stretching modes of thiophene through introduction of an S–I_2 bond.[32,33] To compare thiophene *versus* furan dyes binding I_2, TiO_2–dye films were prepared with **D35** (thiophene), **AB3** (furan), **LD03** (thiophene) and **LD04** (furan). **AB1** (thiophene) and **AB2** (furan) were not studied *via* Raman spectroscopy since they suffer from decomposition on films in the presence of I_2 alone. Notably, **AB1** and **AB2** were stable in operational DSC devices presumably due to the full electrolyte stabilizing the dyes. For the other 4 dyes, Raman spectra were collected on the TiO_2–dye films with and without I_2 in the common DSC device electrolyte solvent MeCN. **D35** (thiophene) and **AB3** (furan) both show an increase in the relative intensity of the peaks seen between 1000–1600 cm^{-1} when compared with the 300–1000 cm^{-1} region; however, the increase is substantially greater for **D35** (thiophene) (Fig. 3a and b). Initial pure dye peaks and new peaks associated with I_2 addition can be seen around 950 cm^{-1}, 1025 cm^{-1}, 1060 cm^{-1}, and 1400–1600 cm^{-1} for **AB3** (furan) (Fig. 3b), but **D35** (thiophene) shows few original dye peaks after I_2 addition with numerous intense signals being added from 1000–1600 cm^{-1} (Fig. 3a). This points to the presence of iodine binding in both dyes, however the presence of the sulfur atom in **D35** (thiophene) has resulted in a larger change in the Raman spectrum relative to **AB3** (furan). This larger change in the **D35** (thiophene) Raman spectrum is the result of a single atom change from oxygen in **AB3** (furan) to a sulfur. Given that the experimental conditions were held constant, this single atom is responsible for the large change in the Raman spectrum when I_2 is present. The changes are consistent with a sulfur–halogen bonding event to I_2 as discussed in the computational section below.

To reduce the possible influence of the nitrogen atom of the amine donor during these studies, the simple alkoxy donor-based dyes, **LD03** (thiophene) and **LD04** (furan), were examined in an identical study. Changes in the Raman spectra were subtler for these two derivatives which could be due to the absence of nitrogen–I_2 interactions or due to a less electron rich thiophene binding weaker to I_2 when only a relatively weak

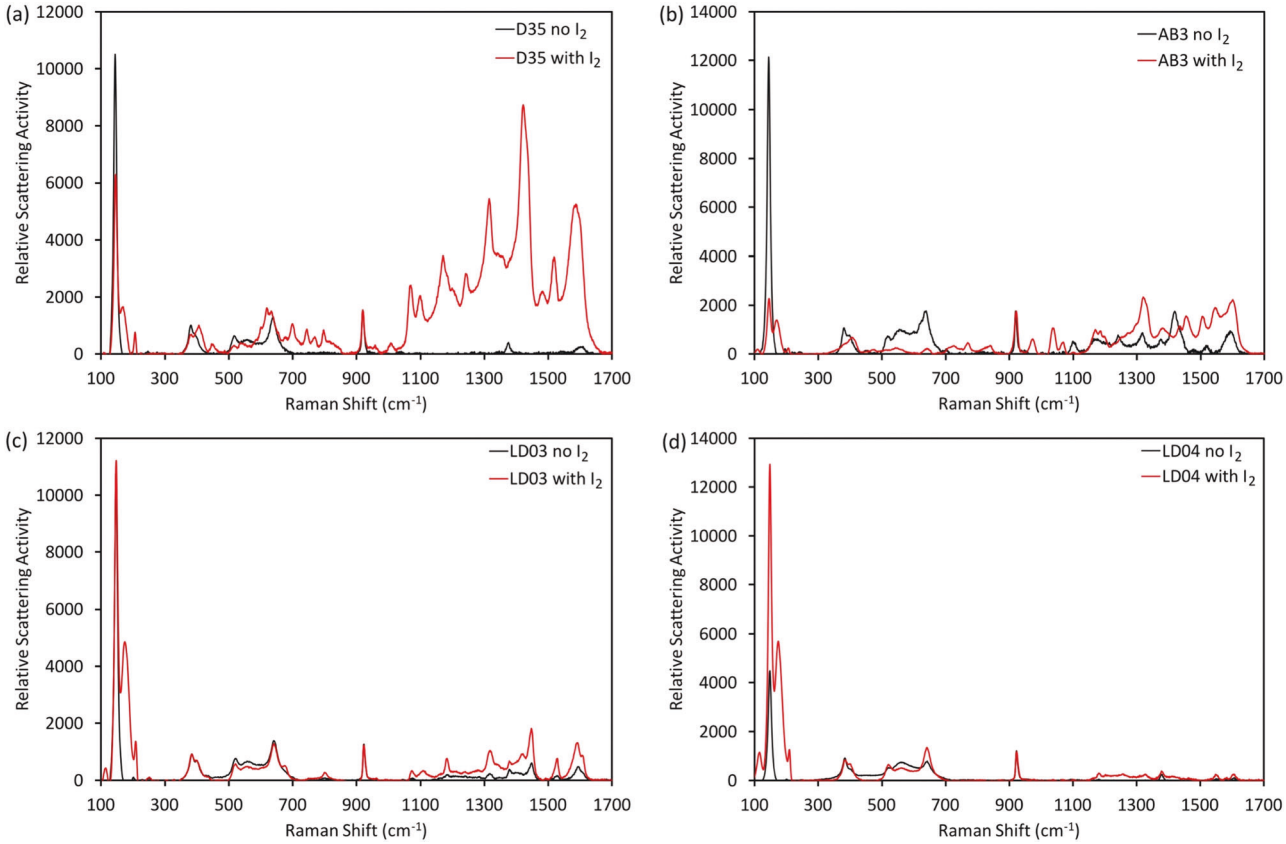

Fig. 3 Raman spectra for (a) **D35**, (b) **AB3**, (c) **LD03** and (d) **LD04** on TiO_2 films under acetonitrile with and without I_2 present. Background spectrum were subtracted in each case without the dye present but all other components were present.

ether donor is used. A larger difference in the relative intensity of the peaks between 1000–1600 cm^{-1} with and without I_2 present is observed for **LD03** (thiophene, Fig. 3c) when compared with the 300–1000 cm^{-1} region, while the change for **LD04** (furan, Fig. 3d) is less dramatic when these regions are compared. These results indicate a difference in the influence of I_2 on the Raman spectrum of **LD03** (thiophene) when compared to **LD04** (furan) which may be attributed to the stronger binding of I_2 by thiophene. This observation is consistent with Raman spectroscopy studies performance on films of **D35** (thiophene) and **AB3** (furan).

Computational analysis

To gain insight into the changes observed experimentally in the Raman spectra, the interactions of **AB1** (thiophene), **AB2** (furan), **D35** (thiophene) and **AB3** (furan) with I_2 were probed computationally to examine the hypothesis of thiophene interacting non-covalently with I_2 more strongly than furan. **AB1** (thiophene) and **AB2** (furan) were also of interest since spectroscopic film studies in the presence of I_2 could not be conducted. Since **LD03** (thiophene) and **LD04** (furan) displayed similar Raman spectra trends to **D35** (thiophene) and **AB3** (furan), the more common benchmark dye **D35** (thiophene) was chosen for computational studies to compare with analogue **AB3** (furan). First, geometries of the dyes were optimized in two different conformations (referred to as *cis* and *trans* based on the

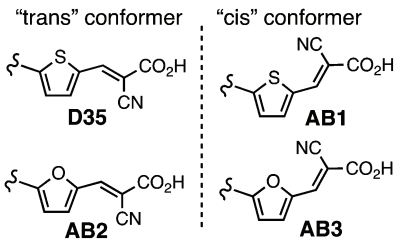

Fig. 4 Illustration of the *trans* and *cis* conformer assignments.

orientation of the CN group of the cyanoacrylic acid relative to the thiophene sulfur or furan oxygen atoms, Fig. 4) in isolation without I_2 present at the wB97XD/6-31+G* level of theory. On TiO_2 film surfaces the exact dye geometry is challenging to predict, thus two geometries were analyzed for the four dyes examined. Calculations were conducted in the absence of solvent and the TiO_2 surface to reduce the complexity in trying to evaluate vibrational changes induced by non-covalent bonding with a large number of atoms present.

To examine the dye interactions of I_2 at the thiophene or furan rings, I_2 was positioned near the heterocycles of the geometry optimized dyes in space with a linear orientation of I_2 and the S/O atom all in the same plane as the heterocycle. The geometries were then optimized to the lowest energy conformation. It is noteworthy that a number of binding sites

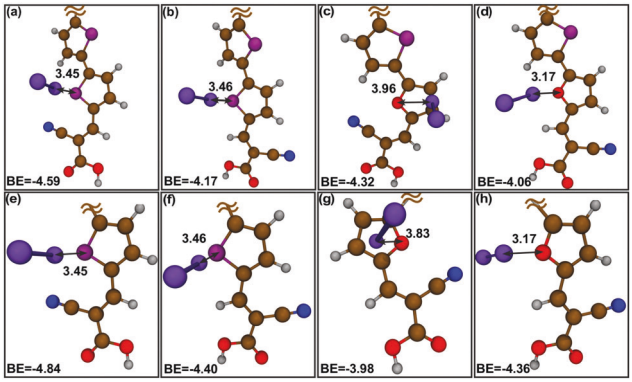

Fig. 5 Illustration of the closest I_2 binding energy minima at the heterocycle near that CAA acceptor for *cis*-**AB1**, *trans*-**AB1**, *cis*-**AB2**, *trans*-**AB2**, *cis*-**D35**, *trans*-**D35**, *cis*-**AB3**, and *trans*-**AB3**. Calculations were done at wB97XD/6-31+G* level of theory and basis set.

Table 1 Computational results for I_2 binding distance, binding energies and dihedral angles at wB97XD/6-31+G* level

Dye	S/O–I_2 distance (Å)	Binding energy (kcal mol^{-1})	S/O–I_2 dihedral (°)
cis-**AB1** (thiophene)	3.45	−4.59	81
trans-**AB1** (thiophene)	3.46	−4.17	71
cis-**AB2** (furan)	No minimum	No minimum	—
trans-**AB2** (furan)	3.17	−4.06	65
cis-**D35** (thiophene)	3.45	−4.84	81
trans-**D35** (thiophene)	3.46	−4.40	70
cis-**AB3** (furan)	No minimum	No minimum	—
trans-**AB3** (furan)	3.17	−4.36	70

are evident on each dye with stronger binding at the nitrogen atoms of the triarylamine and cyanoacrylic acid; however, these binding events are present in all dyes. We have focused on the heterocycles as these binding events differentiate the thiophene and furan dyes. A close interaction for sulfur and iodine of ~3.45 Å is observed for *cis*- or *trans*-**AB1** (thiophene) with an end-on binding to I_2 at the presumed sigma-hole location (Fig. 5 and Table 1). When comparing these results to **AB2** (furan) it is interesting that only one conformer (*trans*) binds I_2 to give a linear O–I_2 geometry orientation. The *cis*-**AB2** (furan) conformer does not show an energy minimum with a linear geometry, but instead the I_2 shifts to above the π-face of the system as the nearest energy minimum (Table 1 and Fig. 5). This result supports our experimental finding that sulfur of thiophene binds I_2 stronger than the oxygen of furan, since one of the potential binding sites for furan is non-active in the *cis* conformation. For the cases where I_2 adopts a linear orientation relative to the sulfur and oxygen atoms, the I_2 molecule adopts a 65° to 81° dihedral angle with the π-system of the heterocycle (Fig. 5 and Table 1). Similar results are observed when the *trans* and *cis* isomers of **D35** (thiophene) and **AB3** (furan) are compared. For the comparable *trans* isomers, the location of the highest occupied molecular orbital (HOMO) and the lowest unoccupied molecular orbital (LUMO) offer some insight into the nature of this binding event. The HOMO of *trans*-**D35** (thiophene) and *trans*-**AB3** (furan) is delocalized onto

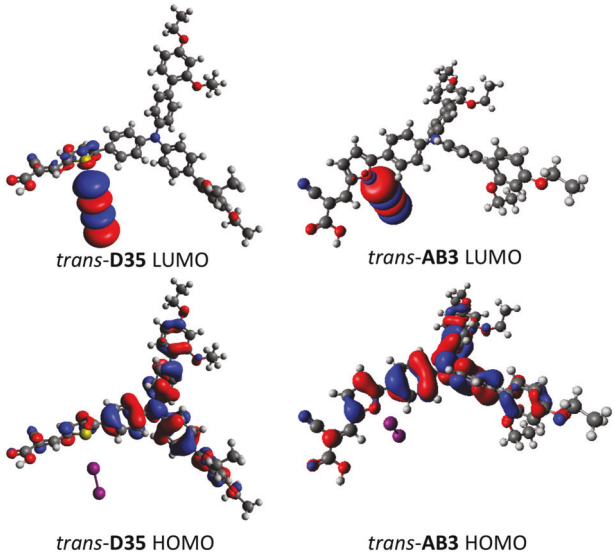

Fig. 6 HOMO and LUMO orbitals of *trans* **D35** and **AB3**. Calculations were done at wB97XD/6-31+G* level of theory and basis set. Iso values are set to 0.2.

the heterocycles (Fig. 6, see ESI† for **AB1** and **AB2** orbitals). In both cases the LUMO is heavily localized on the I_2 molecule suggesting an intermolecular charge transfer event may be possible. This interaction is indicative of a halogen bonding event in a conformation that would be predicted by a first principle approximation.

Binding energies were analyzed for these dyes to I_2 by summing the energies of the dye and I_2 separately optimized in isolation, then comparing with the system energy having both the dye and I_2 present. Again, only the *trans* isomers could be compared as no *cis*-**AB2** (furan)–I_2 optimized geometry could be located which was comparable to thiophene analogue (Table 1). The *trans*-**AB1** (thiophene)–I_2 binding energy was found to be stronger than that of the *trans*-**AB2** (furan)–I_2 binding energy by a 0.11 kcal difference. A very similar analysis can be made comparing **D35** (thiophene) and **AB3** (furan), with **AB3** (furan) again showing no binding in a linear orientation to I_2 for the *cis* conformer and the *trans* conformer showing weaker binding relative to the *trans*-**D35** (thiophene) analogue (Fig. 6 and Table 1). When the *cis* and *trans* isomers are compared for the thiophene based dyes **AB1** and **D35**, a 0.42–0.44 kcal mol^{-1} greater binding energy is present for the *cis* isomers. Thus, not only do thiophene-based dyes have a stronger analogue binding mode than the furans in the *trans* conformation, but they also bind even stronger in the *cis* conformation which is exclusive to thiophene. These results suggest that an I_2 binding event may not be completely absent from furan heterocycles, but thiophene analogues exhibit much stronger halogen bonding interactions in multiple conformations.

Having found optimized geometries for **D35** (thiophene) and **AB3** (furan) with and without I_2, we simulated Raman spectra from DFT calculations at the wB97XD/6-31+G* level of theory to better understand the vibrational modes in the 1400–1800 cm^{-1} range of the experimental Raman spectrum which were

changing much more dramatically for **D35** (thiophene) in the presence of I_2 relative to **AB3** (furan, Fig. 3 and Fig. S1, ESI†). Two different geometries for each dye were analyzed with and without I_2 present. While the simulated spectra can be used to help understand the experimental spectra, a direct comparison cannot be made since the simulated Raman spectra is obtained in the gas phase with only one I_2 molecule present and under harmonic approximations while the experimental data was collected on the surface with acetonitrile solvent present with a large excess of I_2 molecules. Thus, the comparison of the data is restricted to broad wavenumber ranges rather than to wavenumber peaks. It could be seen that in both the *cis* and *trans* conformations for **AB3** (furan) no shift or emergence of new peaks can be seen when I_2 is present and only a slight change in intensities for 2–3 peaks between 1500–1700 cm^{-1} is observed (Fig. S1, ESI†). However, in terms of **D35** (thiophene), the *cis* conformation shows a slight change in intensity along with a shifting of peaks between 1500–1600 cm^{-1} by 3–5 cm^{-1} toward higher energy, while the *trans* conformation shows intensity changes and some shifting of peaks near 1100 and 1600 cm^{-1} with a new peak at $\sim$1250 cm^{-1} evident (Fig. S1, ESI†). For the DFT Raman spectra, the 1500–1600 cm^{-1} region where the most significant changes occur corresponds to ring breathing and stretching modes for both thiophene and furan. Experimentally, the largest changes in the Raman spectrum are occurring near this region as well. Given that the experimental changes when I_2 is present were significantly more pronounced for the thiophene based dyes, this suggests that I_2 is interacting stronger with thiophene resulting in significant changes in ring breathing/stretching modes for this heterocycle but to a lesser extent for furan. It is reasonable that the presence of this interaction for thiophene is due to halogen bonding from the sulfur atom to I_2.

UV-Vis absorption spectroscopy

To further evaluate our hypothesis that the sulfur of thiophene binds I_2 more strongly than the oxygen of furan, we measured film UV-Vis absorption spectra for **D35** (thiophene), **AB3** (furan), **LD03** (thiophene) and **LD04** (furan). We reasoned that if I_2 binding were occurring with thiophene effects should also be visible in the UV-Vis spectrum. A S–I_2 halogen bond would be predicted to red-shift the dye absorption spectrum since the I_2 serves as an electron acceptor which would lower the LUMO energy based on first approximations. Therefore, we predict significant observable changes in dye absorption transition energies for the thiophene-based dyes **D35** and **LD03** due to S–I_2 binding and relatively minor changes for the furan-based dyes **AB3** and **LD04** due to a weaker O–I_2 interaction. To probe this prediction, we prepared TiO_2 films of each of the dyes and submerged them in solutions of acetonitrile with and without I_2 present. The UV-Vis spectra were analyzed by comparing the shift in the λ_{max} and shape of the normalized absorption curves. On TiO_2 films submerged in acetonitrile with and without I_2, the λ_{max} of **D35** (thiophene) shifts about 10 nm, while the λ_{max} of **AB3** (furan) shows no shift (Fig. 7). For the simple alkoxy donor dyes, **LD03** (thiophene) shows a 7 nm shift

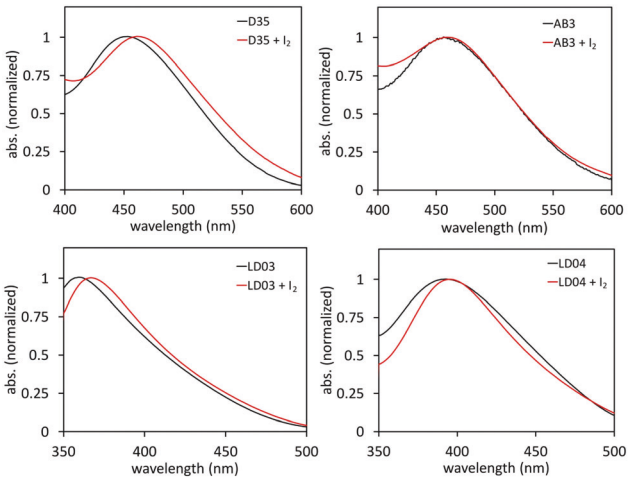

Fig. 7 UV-Vis absorption spectra for dyes **D35**, **AB3**, **LD03**, and **LD04** in acetonitrile with and without I_2 present on films. Background spectrum were subtracted in each case without the dye present but all other components were present.

in the λ_{max} value, while **LD04** (furan) shows a smaller 3 nm shift (Fig. 7). The larger shift in λ_{max} for the thiophene based dyes can be attributed to a halogen bonding event due to the presence of I_2 binding stronger with the sulfur atom in thiophene than the oxygen of furan. Additionally, the shift toward lower energy photon absorption (red-shift) in the presence of I_2 occurs as predicted. This is consistent with the hypothesis that halogen bonding with thiophene and I_2 is occurring by donation of electron density from the sulfur to I_2.

To computationally probe the experimentally observed changes in the UV-Vis spectrum in the presence of I_2, time dependent-density functional theory (TD-DFT) calculations were undertaken to evaluate which orbitals were contributing to the observed red-shift and to identify the position of these orbitals. If I_2 binding is causing the red-shift, a low energy transition of electron density from the dye to I_2 is predicted. To evaluate this prediction, the first 10 states were examined using the previously optimized geometries (both *cis* and *trans* for each dye) for **AB1** (thiophene), **AB2** (furan), **D35** (thiophene), and **AB3** (furan) with TD-DFT calculations at the wB97XD/6-31+G* level of theory. For all of the dyes, in the presence of I_2 the first two states have very low oscillator strengths (f of $\sim$0.0005) ranging from 0.3 to 0.5 eV lower in energy than the first major transition (Tables S2–S9, ESI†). The transitions for the first two states also involve a large number of orbitals (up to five occupied to unoccupied transitions). The first strong transition (state 3, f of 0.99) for *cis* **AB1** (thiophene) is made up of several transitions from occupied orbitals centered on the dye with no significant concentration on I_2 to unoccupied orbitals localized on I_2. Among the transitions involved in this state, the HOMO–LUMO transition is the strongest contributor at 27% followed by the HOMO−1 to LUMO at 15% with 9 total transitions (Table S2 and Fig. S2, ESI†). Compared to the first state (f = 1.7, primarily HOMO to LUMO and HOMO−1 to LUMO) of *cis* **AB1** (thiophene) in the absence of I_2, state 3 of *cis* **AB1** (thiophene) with I_2 is 0.14 eV lower in

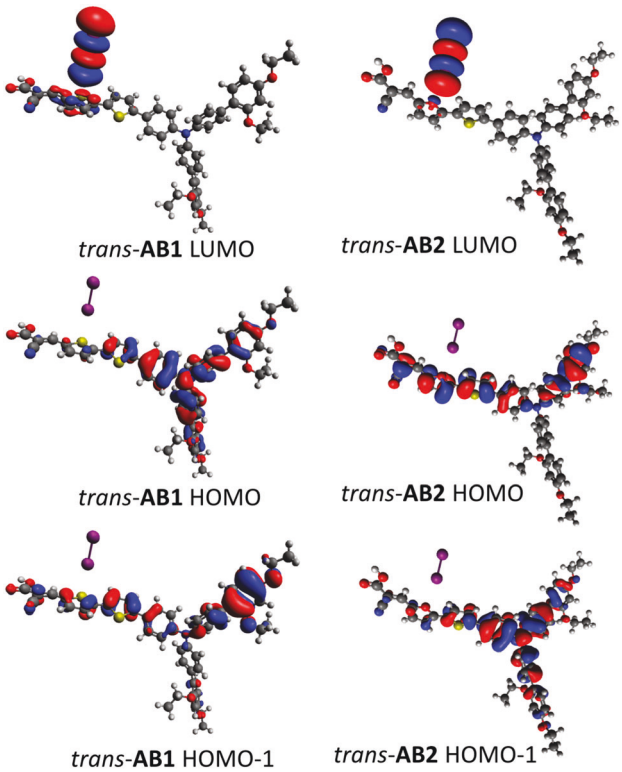

Fig. 8 Orbitals contributing to the first strong oscillator strength state for *trans* **AB3** and **D35**. Calculations were done at wB97XD/6-31+G* level of theory and basis set.

energy. Analysis of *trans* **AB1** (thiophene) with and without I_2 reveals a very similar set of observations (Fig. 8 and Fig. S3, Table S3, ESI†). As noted previously, the geometry minima for *cis* **AB2** (furan) is significantly different. However, for both *cis* and *trans* isomers of **AB2** (furan), the first two states show very weak oscillator strengths, and the first major oscillator strength observed is for state 3 when I_2 is present. State 3 for *cis* **AB2** (furan) is still comprised of the same dominant orbital transitions as *cis* **AB1** (thiophene) (HOMO to LUMO and HOMO−1 to LUMO, Table S4 and Fig. S4, ESI†) and a similar magnitude red-shift, but with fewer transition (5 *versus* 9). Interestingly, the oscillator strength for the third state is significantly lower in strength for *cis* **AB2** (furan) than for *cis* **AB1** (thiophene) (0.15 *versus* 0.99). This again suggests a significantly stronger interaction of I_2 with thiophene than furan and supports a S–I_2 halogen bonding hypothesis. *trans* **AB2** (furan) follows the same analysis as *cis* **AB2** (furan) only with a dramatically lower oscillator strength for state 3 (f = 0.02, Fig. 8 and Fig. S5, Table S5, ESI†). This data suggests a very weak interaction between the furan heterocycle and I_2 presumably due to the lack of a significant halogen bonding event between O and I_2. These weak red-shifted transition oscillator strengths for **AB2** (furan) in the presence of I_2 are consistent with the relatively minor changes observed by experimental UV-Vis spectroscopy for the furan-based dyes (**AB3** and **LD04**). Computationally, **AB1** (thiophene) shows a much stronger red-shifted transition oscillator strength in the presence of I_2 which is consistent with the experimental data for the thiophene dyes (**D35** and **LD03**) showing a significant red-shift of the UV-Vis spectrum in the presence of I_2. Computationally, both *cis* and *trans* isomers of **D35** (thiophene) and **AB3** (furan) follow a similar trend to that described above for **AB1** (thiophene) and **AB2** (furan) (Tables S6–S9, ESI†). The experimental and computational data is again consistent with a stronger S–I_2 halogen bonding event than O–I_2.

Device data

Given the spectroscopic observations from the surface Raman studies and film UV-Vis studies, several predictions about the performance of the furan-based and thiophene-based dyes in DSC devices can be made based on the cascade of electron transfer events after photoexcitation of the dye. After the injection of an electron from the photoexcited dye into the TiO_2 CB (eqn (1)), the ground-state dye can be regenerated with iodide (eqn (2)). Although a number of possible electron transfer pathways exist concerning the iodide redox shuttle,[34] a commonly cited pathway suggests the I_2^- product from eqn (2) can then undergo disproportionation to give I_3^- and I^- *via* eqn (3). I_3^- represents the fully oxidized redox shuttle species in DSC devices and is involved with an equilibrium reaction to give I_2 and I^- *via* eqn (4). Thus, I_2 is both continuously being generated within the DSC cell under operational conditions and is explicitly added to the electrolyte to generate a concentration of the triiodide species in solution needed for rapid electron collection at the counter electrode. The electrons injected into the TiO_2 CB can either traverse an external circuit to the counter electrode as desired before following the reverse reactions eqn (3) and the reduction of I_2^- *via* eqn (5) to give the original iodide reductant, or these electrons can be transferred to an oxidizing species directly from the TiO_2 CB undesirably (eqn (6)). Specifically, the recombination rate of electrons in the TiO_2 semiconductor conduction band (CB) with the redox shuttle should be slower for the furan-based dyes compared with the thiophene-based analogues if the sulfur of thiophene is halogen bonding to I_2 near the TiO_2 surface. The rate of this recombination is a function of distance for the through-space electron transfer, and sulfur halogen bonding with I_2 will increase the local concentration of I_2 near the TiO_2 surface to promote the undesirable electron transfer shown in eqn (6):

$$\text{dye}^* + TiO_2 \rightarrow \text{dye}^+ + TiO_2(e^-) \quad (1)$$

$$\text{dye}^+ + 2I^- \rightarrow \text{dye} + I_2^- \quad (2)$$

$$2I_2^- \rightarrow I_3^- + I^- \quad (3)$$

$$I_3^- \rightleftharpoons I_2 + I^- \quad (4)$$

$$I_2^- + e^- \rightarrow 2I^- \quad (5)$$

$$I_2 + TiO_2(e^-) \rightarrow I_2^- + TiO_2 \quad (6)$$

Since eqn (6) represents a non-productive DSC device electron transfer pathway, it will lower photocurrent because fewer electrons are traveling the external circuit. Additionally, the electron transfer event represented by eqn (6) will also lower photovoltage since electrons are being transferred out of TiO_2

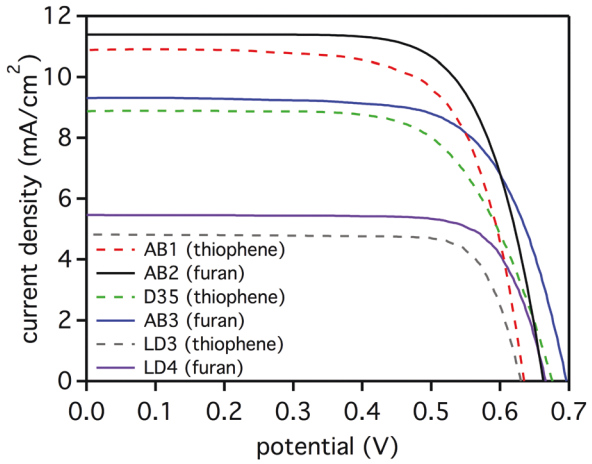

Fig. 9 *J–V* curve comparison for **AB1**, **AB2**, **AB3**, **D35**, **LD03** and **LD04**.

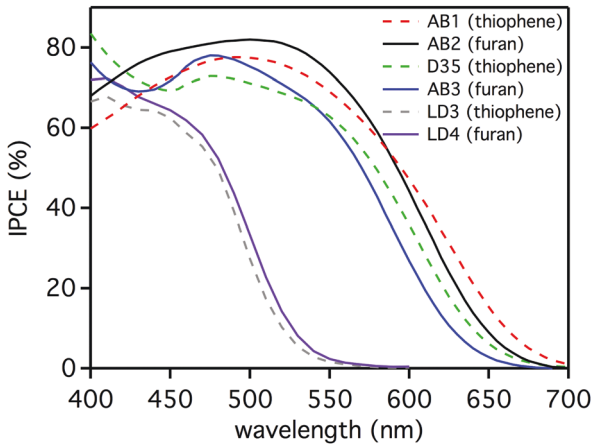

Fig. 10 IPCE curves for **AB1**, **AB2**, **D35**, **AB3**, **LD03**, and **LD04**.

more rapidly leading to a depletion of the number of electrons in the TiO_2 CB and lowering the TiO_2 Fermi level. These predictions can all be tested through a series of DSC device measurements including current–voltage (*J–V*) curve, incident photon-to-current conversion efficiency (IPCE), and small modulation photovoltage transient measurements.

First device performances were analyzed for all of the dyes *via J–V* curve measurements (Fig. 9 and Table 2). In all cases, the furan-based dyes (**AB2**, **AB3**, **LD04**) gave both higher current and voltage than the thiophene analogues (**AB1**, **D35**, **LD03**) as is predicted if a S–I_2 halogen bonding event were occurring. The open-circuit voltage (V_{oc}) values averaged 28 mV higher and the short-circuit current density (J_{sc}) values averaged 0.5 mA cm^{-2} higher for the furan derivatives. *Via* the equation PCE = $(V_{oc} \times J_{sc} \times FF)/I_0$, where FF is fill-factor and I_0 is the sun intensity (set to 1 for this study), the furan-based dyes were found to average 0.6% higher in PCE. This equates to a >10% overall gain in performance for the furan-based dyes when compared with the thiophene-based dyes. Upon analysis of the IPCE spectrum, thiophene based dyes **AB1** and **D35** are significantly red-shifted relative to the furan analogues (**AB2** and **AB3**, respectively); however, the peak IPCE value for the furan analogues is significantly higher which explains the observed photocurrents *via* the *J–V* curve measurements (Fig. 10). The red-shift of the IPCE spectrum is similar to that observed in the UV-Vis measurements for **D35** (thiophene) when I_2 was added. It is noteworthy, that there is little change in the dye–film absorption spectrum under pure acetonitrile when **D35** (thiophene) and **AB3** (furan) absorption spectrum are compared (Fig. 7). As hypothesized for the UV-Vis data explanation, the IPCE red-shift from the furan dyes can be rationalized as I_2 binding to the thiophene containing dyes to remove electron density from the π-system and lowering the LUMO energy of the system. Having I_2 coordinate to the sulfur in thiophene results in electron density being pulled out of the system, effectively lowering the LUMO of the dye and shrinking the HOMO–LUMO gap as was shown *via* TD-DFT above. This causes the thiophene-based dyes IPCE's to be selectively red-shifted relative to the film absorption spectrum. For the **LD03** (thiophene)/**LD04** (furan) comparison, the IPCE onset values are similar, but the furan derivative again shows a higher peak performance. The relative increased peak IPCE performance is consistent with the S of thiophene halogen bonding to I_2 to promote unwanted recombination, while a significantly weaker interaction (if any) is present for the O of furan with I_2 which does not promote recombination.

Table 2 Device parameters for **AB1**, **AB2**, **AB3**, **D35**, **LD03** and **LD04**

Dye	V_{oc} (mV)	J_{sc} (mA cm^{-2})	FF	PCE (%)	Dye loading (mol cm^{-2})
AB1 (T)	631	11.0	0.65	4.6	2.49×10^{-7}
AB2 (F)	659	11.4	0.71	5.5	2.50×10^{-7}
D35 (T)	675	8.9	0.64	3.9	3.53×10^{-8}
AB3 (F)	696	9.4	0.67	4.5	4.62×10^{-8}
LD03 (T)	630	4.8	0.77	2.4	1.87×10^{-7}
LD04 (F)	664	5.5	0.76	2.8	1.20×10^{-7}

See device fabrication section for TiO_2 thicknesses and compositions. Dyes were deposited from a THF : EtOH (1 : 4) solution with a dye concentration of 0.3 mM and a 40 : 1 CDCA : dye ratio overnight in the dark at room temperature. The electrolyte was composed of 0.1 M GuCNS, 1.0 M DMII, 0.03 M I_2, 0.5 M TBP and 0.05 M LiI in 85 : 15 MeCN : valeronitrile. T = thiophene. F = furan.

To better understand the rate of recombination of electrons in the TiO_2 CB with I_2 (eqn (6)), electron lifetime measurements were made *via* small modulated photovoltage transient studies (Fig. 11). Given the larger V_{oc} and J_{sc} values for the furan-based dyes, longer electron lifetimes are expected for **AB2** (furan), **AB3** (furan), and **LD04** (furan) than the thiophene analogues. This is indeed the case, with **AB2** (furan) and **LD04** (furan) showing dramatically longer electron lifetimes than **AB1** (thiophene) and **LD03** (thiophene) (Fig. 11). Even for the case of the exceptionally long electron lifetime benchmark dye **D35** (thiophene), the furan analogue **AB3** shows a longer electron lifetime. These results add further evidence that the sulfur of thiophene is halogen bonding with I_2 near the TiO_2 surface to promote a faster electron recombination event.

Since V_{oc} and J_{sc} device performance metrics are often correlated to dye loadings, dye desorption studies were conducted to probe if dye loading could have had a significant influence in the device data results in addition to the stronger halogen bonding of thiophene relative to furan (Table 2).

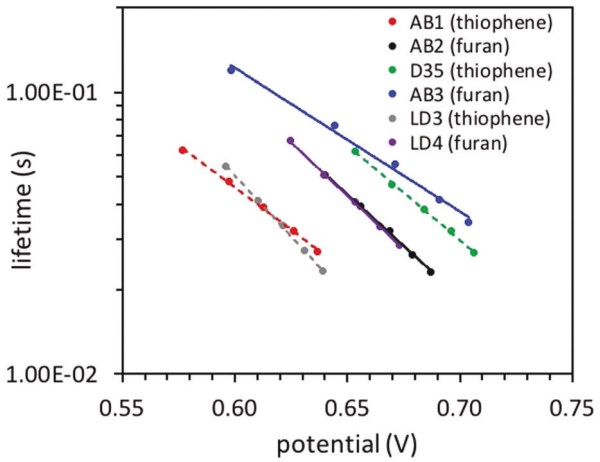

Fig. 11 Electron lifetime measurements for dyes **AB1**, **AB2**, **AB3**, **D35**, **LD03** and **LD04** using small modulation photovoltage transient measurements.

While the dye analogues only differ by a single atom, the atom used in the heterocycle has a significant influence on the geometry of the substituents at the 2 and 5 positions of furan or thiophene. The O–C bond lengths are shorter for furan which leads to more of a "U" shape, while the S–C bonds are longer in the case of thiophene which leads to more of a linear geometry. The variation in geometry could result in a difference in dye loading despite the seemingly subtle change of a single atom. However, the dye loadings were all found to be similar between the analogues. Specifically, the dye loadings for **AB1** (thiophene) and **AB2** (furan) were found to be near identical at 2.5×10^{-7} mol cm^{-2}, and **D35** (thiophene) was found to have a dye loading within 25% of the value of **AB3** (furan). Interestingly, the dye loading varied the most between **LD03** (thiophene) and **LD04** (furan) with about 55% more **LD03** (thiophene) in the devices, yet despite the higher dye loadings for the thiophene based dye, the furan-based dye still has a higher photocurrent, photovoltage, and electron lifetime within DSC devices. This highlights that the factors controlling the recombination rate for these systems is certainly more than just a simple surface blocking model dominated by dye loadings. These observations further suggest that the halogen bonding of S to I_2 is a primary factor in the uniformly lower V_{oc} and J_{sc} values of thiophene dyes relative to furan.

Conclusion

Overall, evidence for stronger binding of I_2 to thiophene containing dyes *versus* furan containing dyes is observed. Raman spectroscopy on TiO_2 surface bound dyes shows a much more dramatic change in the intensity and shifting of vibrational peaks in the presence of iodine for thiophene-based dyes **LD03** and **D35** relative to the furan-based analogues **LD04** and **AB3**, respectively. UV-Vis analysis again lends evidence of I_2 binding **LD03** (thiophene) and **D35** (thiophene) on TiO_2 by showing a red shift in the λ_{max}. Indirect evidence of I_2 binding could be seen for **AB1** (thiophene) and **AB2** (furan) where device V_{oc} and J_{sc} measurements show a higher value for the furan-based dye despite identical dye loadings. This suggests a lower recombination rate which was confirmed *via* electron lifetime studies through small modulated photovoltage transient measurements for **AB1** and **AB2**. IPCE measurements also showed a red-shift and decrease in IPCE for thiophene based dyes **AB1** and **D35** similar to the addition of an electron withdrawing group, hinting toward the coordination of I_2 to sulfur lowering the LUMO energy. Computational studies lend further support to these experimental observations as the thiophene based dyes **AB1** and **D35** were both found to have a stronger influence from an I_2 binding mode at the sulfur atom of thiophene than at the oxygen atom of furan for **AB2** and **AB3**, respectively. TD-DFT results reveal that the thiophene based dyes more readily transfer electron density (have a higher oscillator strength) from the dye to I_2 *via* the HOMO centered on the dye and LUMO centered on I_2. The oscillator strengths were significantly lower for the analogous charge transfer event with furan-based dyes. This study shows substantial evidence for I_2 binding to the sulfur atoms of thiophene which means dyes should be carefully designed to reduce S and I_2 interactions near the TiO_2 surface for higher device performances.

Experimental

General experimental details

All commercially obtained regents were used as received. 2′,4′-Dibutoxy-*N*-(2′,4′-dibutoxy-[1,1′-biphenyl]-4-yl)-*N*-(4-(4,4,5,5-tetramethyl-1,3,2-dioxaborolan-2-yl)phenyl)-[1,1′-biphenyl]-4-amine and (*E*)-3-(5-(4-(bis(2′,4′-dibutoxy-[1,1′-biphenyl]-4-yl)amino)-phenyl)thiophen-2-yl)-2-cyanoacrylic acid (D35) were purchased from Dyenamo. 5-Bromofuran-2-carbaldehyde was purchased from ArkPharm. Thin-layer chromatography (TLC) was conducted with Sorbtech silica XHL TLC plates and visualized with UV. Flash column chromatography was performed with Sorbent Tech P60, 40–63 μm (230–400 mesh). Reverse phase column chromatography was performed with Sorbent Tech C18 P60, 40–63 μm (230–400 mesh). ^{1}H and ^{13}C NMR spectra were recorded on a Bruker Avance-300 (300 MHz) spectrometer and a Bruker Avance-500 (500 MHz) spectrometer and are reported in ppm using solvent as an internal standard ($CDCl_3$ at 7.26 and acetone-d_6 at 2.09). Data reported as s = singlet, d = doublet, t = triplet, q = quartet, p = pentet, m = multiplet, br = broad, ap = apparent, dd = doublet of doublets; coupling constant(s) in Hz. UV spectra were measured with a Cary 5000 UV-Vis-NIR spectrometer with either dichloromethane or 0.1 M Bu_4NOH in DMF solution. Cyclic voltammetry curves were measured with a C–H Instruments electrochemical analyzer CHI600E. (*E*)-3-(5′-(4-(Bis(2′,4′-dibutoxy-[1,1′-biphenyl]-4-yl)-amino)phenyl)-[2,2′-bithiophen]-5-yl)-2-cyanoacrylic acid (**AB1**), (*E*)-2-cyano-3-(5-(4-(hexyloxy)phenyl)thiophen-2-yl)acrylic acid (**LD03**) and (*E*)-2-cyano-3-(5-(4-(hexyloxy)phenyl)furan-2-yl)acrylic acid (**LD04**) were synthesized according to literature procedures.[29,30]

Raman experimental details

A Horiba Scientific LabRAM HR Evolution Raman Spectroscopy system was used for the acquisition of Raman spectra. The 633 nm

line from a HeNe laser was focused onto solid samples using a 100× objective with a 0.9 NA and a 1800 grooves per mm grating and CCD camera were used for detection.

Computational details

All geometry optimization and binding energy calculations were completed with Gaussian 16 package.[35] wB97XD functional[36] was used to include long-range corrections with D2 dispersion model.[37] Tight optimization criteria were used for both force and density matrix convergence along with ultrafine grid for numerical integration. We used a 6-31+G* basis set for all atoms except for I, where we used LANL2DZdp[38,39] basis set and associated effective core potential. Each dye molecules consists of two different configurations; *cis*- and *trans*-, which are defined as whether the S (for thiophene ring) and O (for furan ring) were on the same or on the different side of N (for nitrile functional group). For the binding energy calculations, 5 (five) different sites were considered for **AB1** and **AB2**; however, in case of **AB3** and **D35**, 4 (four) different sites were considered. In each of these sites, the I_2 molecule was placed at 4 different locations around the considered sites to account for the variations in binding energy. Frequency calculations indicate all geometries are in their corresponding local minima's.

Synthetic protocols

5-(5-(4-(Bis(2′,4′-dibutoxy-[1,1′-biphenyl]-4-yl)amino)phenyl)-thiophen-2-yl)furan-3-carbaldehyde. In a 8.0 mL glass vial, 2′,4′-dibutoxy-*N*-(2′,4′-dibutoxy-[1,1′-biphenyl]-4-yl)-*N*-(4-(4,4,5,5-tetramethyl-1,3,2-dioxaborolan-2-yl)phenyl)-[1,1′-biphenyl]-4-amine (75 mg, 0.092 mmol), 5-(5-bromothiophen-2-yl)furan-2-carbaldehyde[40] (22 mg, 0.084 mmol) and potassium phosphate (53 mg, 0.25 mmol) were dissolved in 1.68 mL of toluene and 0.073 mL of water. The solution was then degassed for about 10 minutes under nitrogen, after which $Pd_2(dba)_3$ (3.0 mg, 0.003 mmol) and XPhos (6.0 mg, 0.013 mmol) were added together. The reaction was then sealed, and brought to 80 °C for 15 hours. The reaction was then removed from heat and cooled to room temperature. The mixture was then extracted with ethyl acetate and water and dried with magnesium sulfate. The crude product was purified with silica gel chromatography with a gradient from 10% ethyl acetate/hexanes to 20% ethyl acetate/hexanes (0.076 g; 95% yield). ^{1}H NMR (500 MHz, acetone-d_6) δ 9.66 (s, 1H), 7.71 (d, J = 8.7 Hz, 2H), 7.66 (d, J = 3.9 Hz, 1H), 7.60–7.55 (m, 5H), 7.51 (d, J = 3.9 Hz, 1H), 7.32 (d, J = 8.4 Hz, 2H), 7.21 (d, J = 8.6 Hz, 4H), 7.18 (d, J = 8.7 Hz, 2H), 7.03 (d, J = 3.8 Hz, 1H), 6.68 (d, J = 2.3 Hz, 2H), 6.64 (dd, J = 2.4, 2.4 Hz, 2H), 4.13–4.04 (m, 8H), 1.85–1.73 (m, 8H), 1.62–1.46 (m, 8H), and 1.05–0.95 (m, 12H) ppm. ^{13}C NMR (500 MHz, $CDCl_3$) δ 176.9, 159.7, 157.1, 155.2, 151.5, 148.4, 147.1, 145.5, 133.7, 131.0, 130.4, 129.4, 127.5 (appears broad, assumed 2 signals), 126.9, 126.7, 124.3, 123.3, 123.1, 123.0, 107.3, 105.4, 100.6, 68.3, 67.9, 31.5, 31.3, 19.5, 19.4, 14.0, and 14.0 ppm. IR (neat) ν = 3190, 3073, 3030, 2955, 2926, 2868, 2330, 2117, 1730, 1670, 1599 cm^{-1}. HRMS *m/z* calc'd for $C_{55}H_{59}NO_6SCs$ [M + Cs]$^+$: calculated 994.3118, found 994.3125.

(*E*)-3-(5-(5-(4-(Bis(2′,4′-dibutoxy-[1,1′-biphenyl]-4-yl)amino)-phenyl)thiophen-2-yl)furan-3-yl)-2-cyanoacrylic acid (AB2). In a 8 mL vial, compound 5-(5-(4-(bis(2′,4′-dibutoxy-[1,1′-biphenyl]-4-yl)amino)phenyl)thiophen-2-yl)furan-3-carbaldehyde (0.040 g, 0.047 mmol) was dissolved in 0.94 mL chloroform. The mixture was then degassed with N_2 for approximately 30 minutes. Cyanoacetic acid (0.012 g, 0.14 mmol) and piperidine (0.032 mL, 0.33 mmol) were added to vial, which was then sealed, heated to 90 °C and allowed to stir for 16 hours. The reaction mixture was diluted with dichloromethane and purified through a plug of silica gel with 100% dichloromethane to 10% methanol/dichloromethane to 12% methanol/3% acetic acid/dichloromethane. The solvent of the third fraction was evaporated under reduced pressure. The dye was then extracted with hexanes and water to give the final dye (**AB2**, 0.040 g, 91% yield). ^{1}H NMR (500 MHz, acetone-d_6) δ 8.07 (s, 1H), 7.73–7.69 (m, 4H), 7.57 (d, J = 8.6 Hz, 4H), 7.55 (d, J = 3.9 Hz, 1H), 7.32 (d, J = 8.4 Hz, 2H), 7.22–7.17 (m, 6H), 7.11 (d, J = 3.7 Hz, 1H), 6.69 (d, J = 2.3 Hz, 2H), 6.64 (dd, J = 2.4, 2.4 Hz, 2H), 4.11–4.00 (m, 8H), 1.85–1.70 (m, 8H), 1.60–1.46 (m, 8H), and 1.05–0.95 (m, 12H) ppm. IR (neat) ν = 3050, 2952, 2924, 2854, 2360, 2340, 1699, 1602 cm^{-1}. ESI HRMS *m/z* calc'd for $C_{58}H_{59}N_2O_7S$ [M − H]$^-$: calculated 927.4043, found 927.4072.

5-(4-(Bis(2′,4′-dibutoxy-[1,1′-biphenyl]-4-yl)amino)phenyl)-furan-2-carbaldehyde. In a 8.0 mL glass vial, 2′,4′-dibutoxy-*N*-(2′,4′-dibutoxy-[1,1′-biphenyl]-4-yl)-*N*-(4-(4,4,5,5-tetramethyl-1,3,2-dioxaborolan-2-yl)phenyl)-[1,1′-biphenyl]-4-amine (100 mg, 0.12 mmol), 5-bromofuran-2-carbaldehyde (20 mg, 0.11 mmol) and potassium phosphate (71 mg, 0.34 mmol) were dissolved in 2.24 mL of toluene and 0.097 mL of water. The solution was then degassed for about 10 minutes under nitrogen, after which $Pd_2(dba)_3$ (4.0 mg, 0.005 mmol) and XPhos (8.5 mg, 0.018 mmol) were added together. The reaction was then sealed, and brought to 80 °C for 15 hours. The reaction was then removed from heat and cooled to room temperature. The mixture was then extracted with ethyl acetate and water and dried with magnesium sulfate. The crude product was purified with silica gel chromatography with 10% ethyl acetate/hexanes (0.092 g; 96% yield). ^{1}H NMR (500 MHz, $CDCl_3$) δ 9.59 (s, 1H), 7.67 (d, J = 8.9 Hz, 2H), 7.47 (d, J = 8.6 Hz, 4H), 7.30 (d, J = 3.8 Hz, 1H), 7.28 (s, 2H), 7.20–7.10 (m, 6H), 6.71 (d, J = 3.7 Hz, 1H), 6.65–6,45 (m, 4H), 4.05–3.85 (m, 8H), 1.85–1.70 (m, 8H), 1.50–1.45 (m, 8H), 1.05–0.90 (m, 12H) ppm. ^{13}C NMR (500 MHz, $CDCl_3$) δ 177.1, 160.4, 160.0, 157.3, 151.9, 149.8, 145.3, 134.4, 131.2 (signal appears larger than expected, assumed 2 signals), 130.7, 126.7, 124.9, 123.1, 122.4, 122.1, 106.6, 105.7, 100.8, 68.5, 68.1, 31.7, 31.5, 19.7, 19.6, 14.2, 14.2 ppm. IR (neat) ν = 3200, 3037, 2957, 2931, 2870, 2360, 2333, 2115, 1672, 1602, 1600 cm^{-1}. ESI HRMS *m/z* calc'd for $C_{51}H_{57}NO_6Cs$ [M + Cs]$^+$: calculated 912.3240, found 912.3235.

(*E*)-3-(5-(4-(Bis(2′,4′-dibutoxy-[1,1′-biphenyl]-4-yl)amino)phenyl)-furan-2-yl)-2-cyanoacrylic acid (AB3). In a 8.0 mL vial, 5-(4-(bis(2′,4′-dibutoxy-[1,1′-biphenyl]-4-yl)amino)phenyl)furan-2-carbaldehyde (0.056 g, 0.072 mmol) was dissolved in 1.50 mL chloroform. The mixture was then degassed with N_2 for approximately 30 minutes. Cyanoacetic acid (0.018 g, 0.217 mmol) and piperidine (0.050 mL, 0.507 mmol) were added to vial, which was then sealed, heated to

90 °C and allowed to stir for 16 hours. The reaction mixture was diluted with dichloromethane and purified through a plug of silica gel with 100% dichloromethane to 10% methanol/dichloromethane to 12% methanol/3% acetic acid/dichloromethane. The solvent of the third fraction was evaporated under reduced pressure. The dye was then extracted with hexanes and water to give **AB3** with trace impurities. The product was then purified using reverse phase column chromatography with a gradient from 10% methanol/acetonitrile to 50% methanol/acetonitrile, then with a CombiFlash R_f^+ chromatography system (RediSep R_f Gold high performance silica gel, 0% methanol/dichloromethane to 10% methanol/dichloromethane) to give the final pure dye (0.014 g, 23%). ^{1}H NMR (500 MHz, $CDCl_3$) δ 7.94 (s, 1H), 7.72 (d, J = 8.8 Hz, 2H), 7.47 (d, J = 8.7 Hz, 4H), 7.28–7.25 (m, 3H), 7.21–7.16 (m, 6H), 6.81 (d, J = 3.8 Hz, 1H), 6.60–6.52 (m, 4H), 4.05–3.95 (m, 8H), 1.85–1.70 (m, 8H), 1.50–1.45 (m, 8H), 1.05–0.90 (m, 12H) ppm. IR (neat) ν = 3340, 2944, 2923, 2854, 2333, 2114, 1602, 1593 cm^{-1}. ESI HRMS m/z calc'd for $C_{54}H_{59}N_2O_7$ $[M + H]^+$: calculated 847.4323, found 847.4347.

Photovoltaic device characterization

Photovoltaic characteristics were measured using a 150 W xenon lamp (Model SF150B, SCIENCETECH Inc. Class ABA) solar simulator equipped with an AM 1.5 G filter for a less than 2% spectral mismatch. Prior to each measurement, the solar simulator output was calibrated with a KG5 filtered monocrystalline silicon NREL calibrated reference cell from ABET Technologies (Model 15150-KG5). The current density–voltage characteristic of each cell was obtained with a Keithley digital source-meter (Model 2400). The incident photon-to-current conversion efficiency was measured with an IPCE instrument manufactured by Dyenamo comprised of a 175 W xenon lamp (CERMAX, Model LX175F), monochromator (Spectral Products, Model CM110, Czerny–Turner, dual-grating), filter wheel (Spectral Products, Model AB301T, fitted with filter AB3044 [440 nm high pass] and filter AB3051 [510 nm high pass]), a calibrated UV-enhanced silicon photodiode reference and Dyenamo issued software.

Photovoltaic device fabrication

For the photoanode, TEC 10 glass was purchased from Hartford Glass. Once cut into 2 × 2 cm squares, the substrate was submerged in a 0.2% Deconex 21 aqueous solution and sonicated for 15 minutes at room temperature. The electrodes were rinsed with water and sonicated in acetone 10 minutes followed by sonication in ethanol for 10 minutes. Finally, the electrodes were placed under UV/ozone for 15 minutes (UV-Ozone Cleaning System, Model ProCleaner by UVFAB Systems). A compact TiO_2 underlayer is then applied by treatment of the substrate submerged in a 40 mM $TiCl_4$ solution in water (prepared from 99.9% $TiCl_4$ between 0–5 °C). The submerged substrates (conductive side up) were heated for 30 minutes at 70 °C. After heating, the substrates were rinsed first with water then with ethanol. The photoanode consists of thin TiO_2 electrodes comprised of a 10 μm mesoporous TiO_2 layer (particle size: 20 nm, Dyesol, DSL 18NR-T) for iodine cells with a 5 μm TiO_2 scattering layer (particle size: >100 nm, Solaronix R/SP). Both layers were screen printed from a Sefar screen (54/137-64 W) resulting in 5 μm thickness for each print. Between each print, the substrate was heated for 7 minutes at 125 °C and the thickness was measured with a profilometer (Alpha-Step D-500 KLA Tencor). The substrate was then sintered with progressive heating from 125 °C (5 minute ramp from r.t., 5 minute hold) to 325 °C (15 minute ramp from 125 °C, 5 minute hold) to 375 °C (5 minute ramp from 325 °C, 5 minute hold) to 450 °C (5 minute ramp from 375 °C, 15 minute hold) to 500 °C (5 minute ramp from 450 °C, 15 minute hold) using a programmable furnace (Vulcan® 3-Series Model 3-550). The cooled, sintered photoanode was soaked 30 minutes at 70 °C in a 40 mM $TiCl_4$ water solution and heated again at 500 °C for 30 minutes prior to sensitization. The complete working electrode was prepared by immersing the TiO_2 film into the dye solution for 16 hours. The solution for all the dyes consists of 0.3 mM dye, with 40× of CDCA (chenodeoxycholic acid) (*i.e.* 40 : 1, CDCA : dye ratio) in (4 : 1) EtOH : THF. For preparing the counter electrode, 2 × 2 cm squares of TEC 7 FTO glass were drilled using Dremel-4000 with a Dremel 7134 Diamond Taper Point Bit from the back side to a taped FTO side. After the tape was removed, the electrodes were washed with water followed by a 0.1 M HCl in EtOH wash and sonication in acetone bath for 10 minutes. The washed electrodes were then dried at 400 °C for 15 minutes. A thin layer of Pt-paste (Solaronix, Platisol T/SP) on TCO was slot printed though a punched tape and the printed electrodes were then cured at 450 °C for 10 minutes. After allowing them to cool to room temperature, the working electrodes were then sealed with a 25 μm thick hot melt film (Meltonix 1170-25, Solaronix) by heating the system at 130 °C under 0.2 psi pressure for 1 minute. Devices were completed by filling the electrolyte through the pre-drilled holes in the counter electrodes and finally the holes were sealed with a Meltonix 1170-25 circle and a thin glass cover slip by heating at 130 °C under pressure 0.1 psi for 25 seconds. Finally, soldered contacts were added with a MBR Ultrasonic soldering machine (model USS-9210) with solder alloy (Cerasolzer wire dia 1.6 mm item # CS186-150). A circular black mask (active area 0.15 cm^2) punched from black tape was used in the subsequent photovoltaic studies.

Electron lifetime measurements

Electron lifetime measurements *via* small modulated photovoltage transient measurements, were carried out with a Dyenamo Toolbox (DN-AE01) instrument and software. The intensity of the LED light source (Seoul Semiconductors, Natural White, S42182H, 450 to 750 nm emission) is varied to modulate the device open-circuit voltage. The biased light intensity was modulated by applied voltages of 2.80, 2.85, 2.90, 2.95, and 3.00 V applied to the LED with the 3.0 V bias approaching 1 sun intensity (97%). The direction of illumination was from the photoanode to the counter electrode, and the device was positioned 5 cm from the LED light source. The voltage rise and decay times are fitted with a Levenberg–Marquardt fitting algorithm *via* LabView, and the electron

lifetime was obtained from the averaging of rise and decay time.

Conflicts of interest

There are no conflicts to declare.

Acknowledgements

AB, HC, MAS, NR and JHD thank NASA for award NNX15AK39A. LEM and NIH thank NSF Award OIA-1539035. JHD and NIH thank NSF Award MRI CHE-1532079. STN and DLW thank NSF CAREER Award CHE-1652094. DFT calculations were performed using supercomputers at the High Performance Computing Collaboratory at Mississippi State University.

Notes and references

1 B. O'Regan and M. Grätzel, *Nature*, 1991, **353**, 737.
2 A. Hagfeldt, G. Boschloo, L. Sun, L. Kloo and H. Pettersson, *Chem. Rev.*, 2010, **110**, 6595.
3 M. Grätzel, *J. Photochem. Photobiol., C*, 2003, **4**, 145.
4 K. Kakiage, Y. Aoyama, T. Yano, K. Oya, J. I. Fujisawa and M. Hanaya, *Chem. Commun.*, 2015, **51**, 15894.
5 H. Cheema and J. H. Delcamp, *ACS Appl. Mater. Interfaces*, 2017, **9**, 3050.
6 A. Listorti, B. O'Regan and J. R. Durrant, *Chem. Mater.*, 2011, **23**, 3381.
7 A. Reynal, A. Forneli, E. Martinez-Ferrero, A. Sánchez-Díaz, A. Vidal-Ferran, B. C. O'Regan and E. Palomares, *J. Am. Chem. Soc.*, 2008, **130**, 13558.
8 K. Hu, H. A. Severin, B. D. Koivisto, K. C. D. Robson, E. Schott, R. Arratia-Perez, G. J. Meyer and C. P. Berlinguette, *J. Phys. Chem. C*, 2014, **118**, 17079.
9 M. Mazloum-Ardakani and A. Khoshroo, *Phys. Chem. Chem. Phys.*, 2015, **17**, 22985.
10 X. Li, A. Reynal, P. Barnes, R. Humphry-Baker, S. M. Zakeeruddin, F. De Angelis and B. C. O'Regan, *Phys. Chem. Chem. Phys.*, 2012, **14**, 15421.
11 B. C. O'Regan, K. Walley, M. Juozapavicius, A. Anderson, F. Matar, T. Ghaddar, S. M. Zakeeruddin, C. Klein and J. R. Durrant, *J. Am. Chem. Soc.*, 2009, **131**, 3541.
12 T. Liu and A. Troisi, *Chem. Phys. Lett.*, 2013, **570**, 159.
13 X. A. Jeanbourquin, X. Li, C. Law, P. R. Barnes, R. Humphry-Baker, P. Lund, M. I. Asghar and B. C. O'Regan, *J. Am. Chem. Soc.*, 2014, **136**, 7286.
14 W. B. Swords, S. J. Simon, F. G. Parlane, R. K. Dean, C. W. Kellett, K. Hu, G. J. Meyer and C. P. Berlinguette, *Angew. Chem., Int. Ed.*, 2016, **55**, 5956.
15 S. J. C. Simon, F. G. L. Parlane, W. B. Swords, C. W. Kellett, C. Du, B. Lam, R. K. Dean, K. Hu, G. J. Meyer and C. P. Berlinguette, *J. Am. Chem. Soc.*, 2016, **138**, 10406.
16 H. Kusama, T. Funaki, N. Koumura and K. Sayama, *Phys. Chem. Chem. Phys.*, 2014, **16**, 16166.
17 H. Kusama and K. Sayama, *Phys. Chem. Chem. Phys.*, 2015, **17**, 4379.
18 M. Pastore, E. Mosconi and F. De Angelis, *J. Phys. Chem. C*, 2012, **116**, 5965.
19 K. C. Robson, K. Hu, G. J. Meyer and C. P. Berlinguette, *J. Am. Chem. Soc.*, 2013, **135**, 1961.
20 D.-M. Gu, J.-Z. Zhang, M. Zhang, Y. Geng and Z.-M. Su, *Dyes Pigm.*, 2016, **132**, 136.
21 M. I. Asghar, J. Halme, S. Kaukonen, N. Humalamäki, P. Lund and J. Korppi-Tommola, *J. Phys. Chem. C*, 2016, **120**, 27768.
22 S. Aghazada, P. Gao, A. Yella, T. Moehl, J. Teuscher, J. E. Moser, M. Gratzel and M. K. Nazeeruddin, *ACS Appl. Mater. Interfaces*, 2016, **8**, 26827.
23 M. Cariello, S. M. Abdalhadi, P. Yadav, J. D. Decoppet, S. M. Zakeeruddin, M. Grätzel, A. Hagfeldt and G. Cooke, *Dalton Trans.*, 2018, **47**, 6549–6556.
24 M. Xie, F.-Q. Bai, J. Wang, C.-P. Kong, J. Chen and H.-X. Zhang, *Comput. Mater. Sci.*, 2016, **111**, 239.
25 H.-B. Li, J.-Z. Zhang, J. Zhang, Y. Wu, Y.-A. Duan, Z.-M. Su and Y. Geng, *J. Mol. Model.*, 2014, **20**, 2309.
26 J. Zhang, H.-B. Li, J.-Z. Zhang, Y. Wu, Y. Geng, Q. Fu and Z.-M. Su, *J. Mater. Chem. A*, 2013, **1**, 14000.
27 M. P. Balanay and D. H. Kim, *Comput. Theor. Chem.*, 2014, **1029**, 1.
28 G. Terraneo, G. Resnati and P. Metrangolo, *Iodine Chemistry and Applications, Iodine and Halogen Bonding*, John Wiley & Sons, 1st edn, 2015, ch. 8.
29 E. Gabrielsson, H. Ellis, S. Feldt, H. Tian, G. Boschloo, A. Hagfeldt and L. Sun, *Adv. Energy Mater.*, 2013, **3**, 1647.
30 J. Luo, Z. Wan, C. Jia, Y. Wang and X. Wu, *Electrochim. Acta*, 2016, **215**, 506.
31 S. M. Feldt, E. A. Gibson, E. Gabrielsson, L. Sun, G. Boschloo and A. Hagfeldt, *J. Am. Chem. Soc.*, 2010, **132**, 16714.
32 P. Deplano, F. A. Devillanova, J. R. Ferraro, F. Isaia, V. Lippolis and M. L. Mercuri, *Appl. Spectrosc.*, 1992, **46**, 1625.
33 G. A. Asseily, R. P. Davies, H. S. Rzepa and A. J. P. White, *New J. Chem.*, 2005, **29**, 315.
34 G. Boschloo and A. Hagfeldt, *Acc. Chem. Res.*, 2009, **42**, 1819.
35 M. J. Frisch, G. W. Trucks, H. B. Schlegel, G. E. Scuseria, M. A. Robb, J. R. Cheeseman, G. Scalmani, V. Barone, G. A. Petersson, H. Nakatsuji, X. Li, M. Caricato, A. V. Marenich, J. Bloino, B. G. Janesko, R. Gomperts, B. Mennucci, H. P. Hratchian, J. V. Ortiz, A. F. Izmaylov, J. L. Sonnenberg, D. Williams-Young, F. Ding, F. Lipparini, F. Egidi, J. Goings, B. Peng, A. Petrone, T. Henderson, D. Ranasinghe, V. G. Zakrzewski, J. Gao, N. Rega, G. Zheng, W. Liang, M. Hada, M. Ehara, K. Toyota, R. Fukuda, J. Hasegawa, M. Ishida, T. Nakajima, Y. Honda, O. Kitao, H. Nakai, T. Vreven, K. Throssell, J. A. Montgomery Jr., J. E. Peralta, F. Ogliaro, M. J. Bearpark, J. J. Heyd, E. N. Brothers, K. N. Kudin, V. N. Staroverov, T. A. Keith, R. Kobayashi, J. Normand, K. Raghavachari, A. P. Rendell, J. C. Burant, S. S. Iyengar, J. Tomasi, M. Cossi, J. M. Millam, M. Klene, C. Adamo, R. Cammi, J. W. Ochterski, R. L. Martin, K. Morokuma, O. Farkas,

J. B. Foresman and D. J. Fox, *Gaussian 16, Revision A.03*, Gaussian, 2016.
36 J. D. Chai and M. Head-Gordon, *Phys. Chem. Chem. Phys.*, 2008, **10**, 6615.
37 S. Grimme, *J. Comput. Chem.*, 2006, **27**, 1787.
38 D. Feller, *J. Comput. Chem.*, 1996, **17**, 1571.
39 K. L. Schuchardt, B. T. Didier, T. Elsethagen, L. Sun, V. Gurumoorthi, J. Chase, J. Li and T. L. Windus, *J. Chem. Inf. Model.*, 2007, **47**, 1045.
40 S. H. Kim and R. D. Rieke, *J. Org. Chem.*, 2013, **78**, 1984.

